$$\eta_m^{(l)}\kappa_{mn}^{(l)}(Im\{\tau_{,n}^{(l)}\}Re\{\tau^{(l)}\} - Re\{\tau_{,n}^{(l)}\}Im\{\tau^{(l)}\}) = \eta_m^{(k)}\kappa_{mn}^{(k)}(Im\{\tau_{,n}^{(k)}\}Re\{\tau^{(k)}\} - Re\{\tau_{,n}^{(k)}\}Im\{\tau^{(k)}\}) \quad (31)$$

Based on Eqs. (28) and (31), Eq. (30) reduces to the form

$$Im\{\lambda\}\sum_{l=1}^{L}\int_{R_l}(\rho c)^{(l)}(Re^2\{\tau^{(l)}\} + Im^2\{\tau^{(l)}\})dV \equiv 0 \quad (32)$$

Now since $(\rho c)^{(l)}$ and the integrals appearing in Eq. (32) are all positive definite, it follows that $Im\{\lambda\} \equiv 0$, hence λ is purely real.

Assuming that Eqs. (13–16) represent Euler equations, the following equivalent variational formulation can be written

$$\lambda = -\sum_{l=1}^{L}\int_{R_l}\kappa_{mn}^{(l)}\tau_{,m}^{(l)}\tau_{,n}^{(l)}dV \Big/ \sum_{l=1}^{L}\int_{R_l}(\rho c)^{(l)}(\tau^{(l)})^2 dV \quad (33)$$

Since both the numerator and denominator appearing in Eq. (33) are positive definite, it follows that all λ are negative definite.

In terms of orthogonality and variational relations given by Eqs. (22) and (33), standard procedures[11] can be used to verify the completeness of the $\tau_p^{(l)}$ eigenfunction set together with convergence characteristics of expansions in terms of these functions. Tacitly assuming that solutions for the eigenvalue problem denoted by Eqs. (13–16) exist, the solution to Eqs. (3–6) can be developed following the classical Sturm-Liouville procedure. Hence, considering that the external conditions, Eqs. (4–6), can be homogenized using standard procedures, Eqs. (3–6) reduce to

in R_l: $$(\kappa_{mn}^{(l)}\tilde{T}_{,n}^{(l)})_{,m} + \tilde{Q}^{(l)} = (\rho c)^{(l)}\tilde{T}_{,t}^{(l)} \quad (34)$$

on ∂R_{lk}: $$\eta_m^{(l)}\kappa_{mn}^{(l)}\tilde{T}_{,n}^{(l)} = \eta_m^{(k)}\kappa_{mn}^{(k)}\tilde{T}_{,n}^{(k)} \quad (35)$$

$$\tilde{T}^{(l)} = \tilde{T}^{(k)} \quad (36)$$

on $\partial R_{l\,\mathrm{ext}}$: $$\eta_m^{(l)}\kappa_{mn}^{(l)}\tilde{T}_{,n}^{(l)} + H^{(l)}\tilde{T}^{(l)} = 0 \quad (37)$$

where $\tilde{T}^{(l)}$ is the reduced temperature and $\tilde{Q}^{(l)}$ is the modified heat generation. To solve Eqs. (34–37), $\tilde{Q}^{(l)}$ and $\tilde{T}^{(l)}(x_1,x_2,x_3,0)$ are expanded as follows

$$\frac{1}{(\rho c)^{(l)}}\tilde{Q}^{(l)} = \sum_{p=1}^{\infty} q_p(t)\tau_p^{(l)} \quad (38)$$

$$\tilde{T}^{(l)}(x_1,x_2,x_3,0) = \sum_{p=1}^{\infty} f_p\tau_p^{(l)} \quad (39)$$

where

$$<q_p,f_p> = \frac{\sum_{l=1}^{L}\int_{R_l}(\rho c)^{(l)} < Q^{(l)}/(\rho c)^{(l)},\ \tilde{T}(o)^{(l)} > \tau_p^{(l)}dV}{\sum_{l=1}^{L}\int_{R_l}(\rho c)^{(l)}\tau_p^{(l)}\tau_p^{(l)}dV} \quad (40)$$

In terms of Eqs. (12, 38, and 39), Eqs. (34–37) reduce to

$$\Gamma_{p,t} - \lambda_p\Gamma_p - q_p = 0 \quad (41)$$

Solving Eq. (41) in terms of the initial condition denoted by Eq. (39) yields

$$\Gamma_p = f_p e^{\lambda_p t} + q_p^* e^{\lambda_p t} \quad (42)$$

where * represents the Faltung. Hence, in terms of Eq. (42) the final solution of Eqs. (34–37) takes the form

$$T^{(l)} = \sum_{p=1}^{\infty}\tau_p^{(l)}(f_p e^{\lambda_p t} + q_p^* e^{\lambda_p t}) \quad (43)$$

Because of the generality of the abovementioned development, for the 1-D case, the results derived herein reduce to the Vodicka-Tittle procedure. In particular, the 3-D piecewise weighted orthogonality relation, Eq. (22), reduces to its 1-D Vodicka-Tittle equivalent. One very important feature of the development given herein is that the eigenvalue problem represented by Eqs. (13–16) can be solved either analytically or numerically. Hence, the powerful finite element procedure can be used to obtain the eigenvalues and eigenfunctions of Eqs. (13–16). Using these together with the expansion denoted by Eq. (43), the solution of Eqs. (3–6) can be developed. In such a case, the number of terms retained in the series, Eq. (43), will depend on the fineness of the element breakdown.

References

[1] Zienkiewicz, O. C., *The Finite Element Method in Engineering Science*, McGraw-Hill, New York, 1971.

[2] Padovan, J., "Analysis of Heat Conduction in Anisotropic Axisymmetric Solids," presented at the 9th Annual Southeastern Seminar on Thermal Sciences, July 26–27, 1973, Old Dominion Univ., Norfolk, Va.

[3] Padovan, J., "Quasi-Analytical Finite Element Procedure for Conduction in Anisotropic Axisymmetric Solids," *International Journal for Numerical Methods in Engineering*, Vol. 8, 1974, pp. 297–312.

[4] Ozisik, M. N., *Boundary Value Problems of Heat Conduction*, International Textbook, Scranton, Pa., 1968.

[5] Vodicka, V., "Warmeleitung in Geschichten Kugel- und Zylinder Korpern," *Schweizer Archv.*, Vol. 10, 1950.

[6] Tittle, C. W., "Boundary Value Problems in Composite Media," *Journal of Applied Physics*, Vol. 36, 1965, pp. 1486–1488.

[7] Carslaw, H. S. and Jaeger, J. C., *Conduction of Heat in Solids*, Oxford University Press, London, 1959.

[8] Goodman, T. R., "The Adjoint Heat-Conduction Problems for Solids," ASTIA-AD254-769, (AFOSR-520), April 1961, Air Force Office of Scientific Research, Wright-Patterson Air Force Base, Ohio.

[9] Padovan, J., "Temperature Distributions in Anisotropic Shells of Revolution," *AIAA Journal*, Vol. 10, No. 1, Jan. 1972, pp. 60–64.

[10] Padovan, J., "Conduction in Anisotropic Composite Slabs and Cylinders," to be presented at the 5th International Conference of Heat Transfer, Sept. 1974, Tokyo, Japan.

[11] Courant, R. and Hilbert, D., *Methods of Mathematical Physics*, Interscience Publishers, New York, 1953.

Raman Scattering Applied to Hypersonic Air Flow

MERVIN E. HILLARD JR.,* E. LEON MORRISETTE,† AND M. LAWRENCE EMORY‡

NASA Langley Research Center, Hampton, Va.

Introduction

AN intimate knowledge of three-dimensional flowfields is necessary to determine the design and performance of future flight vehicles. Standard probing techniques which have been adequate to define simple flowfields are no longer useful when severe streamline curvature exists since the presence of the probe may alter the flowfield and the flow direction is not known a priori. The most desirable probe for three-dimensional flows would be nonintrusive and independent of flow direction; obviously, this describes an optical probing technique. In the present investigation, the Raman scattering technique was used to measure the local static temperature and gas number density over a flat plate in a Mach 5 nozzle of the Langley nozzle test chamber with air as the test gas. While this flowfield is not three-dimensional, the accuracy of the resulting measurements of density and temperature confirm the accuracy of the technique for more complicated flows (as long as the spatial resolution of the sample volume is sufficiently small).

Measurements were made in the inviscid flowfield of a sharp leading-edge flat-plate model at several angles of attack ($-5°$ to $15°$) and over a wide range of tunnel conditions (stagnation pressures P_o from 1.7×10^5 to 2.8×10^6 N/m^2 and stagnation temperatures T_o from 317° to 442°K). The measured values of

Received February 6, 1974.

Index categories: Aerospace Technology Utilization; Lasers; Research Facilities and Instrumentation.

* Aero-Space Technologist, Gas Parameters Measurements Section.

† Aero-Space Technologist, Applied Fluid Mechanics Section. Associate Member AIAA.

‡ Engineering Technician, Gas Parameters Measurements Section.

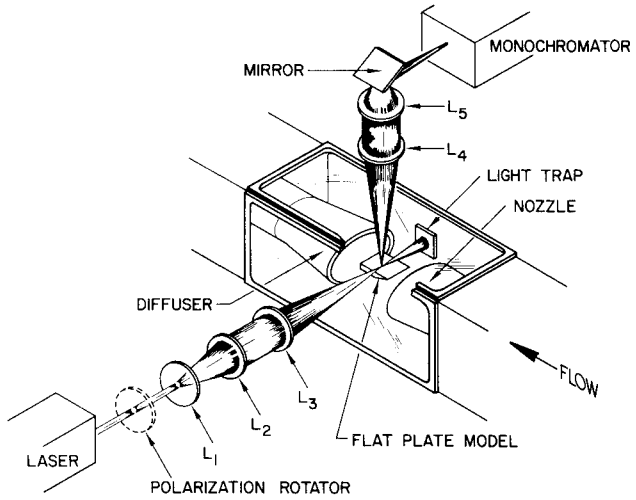

Fig. 1 Experimental setup.

static temperature and density ranged from 60° to 100°K and from 0.03 to 0.8 Kg/m^3, respectively. These values were compared with calculated values based on static pressure measurements along the flat-plate model.

Experimental Apparatus

A schematic diagram of the Raman scattering apparatus is shown in Fig. 1. The exciting radiation was supplied by an argon-ion laser operated at a wavelength of 488 nm (20,492 cm^{-1}) with an output power of 2 w. This radiation was directed to the desired measurement position in the test section by a beam expander (lenses L_1 and L_2) and a focusing lens (L_3). The beam passed through the standard tunnel schlieren window in a single-pass arrangement and was collected in a light trap. The measurement volume was 6 mm in length and 0.1 mm in diameter and was centered on the model centerline 40 mm from the model leading edge and 6 mm above the model; this placed the measurement position approximately 7 mm downstream of the leading-edge shock. The light scattered in the measurement volume was collected perpendicular to the laser beam by lens L_4 ($f/5$), directed into a double monochromator by lens L_5, and detected by a photon-counting system.[1]

The flat-plate model was instrumented with five static pressure orifices placed approximately 13 mm apart along the centerline. In addition, the surrounding chamber pressure, the nozzle-exit static pressure, and the stagnation pressure and temperature were recorded.

The test facility is a 10.7-cm-diam, Mach 5 freejet contained in a chamber. The nozzle is supplied from a high-pressure air tank and exhausts downstream through a diffuser to a vacuum sphere.

Measurement Technique

The Raman effect as discussed by numerous authors[2-4] is an inelastic light-scattering process where the frequency of the scattered light is shifted from that of the incident light by an amount which depends on the structure of the scattering gas molecules. The intensity and intensity variations in the scattered-light spectrum can be directly related to the gas molecular density and temperature.

The static temperature was determined herein by ratioing the intensities of two pure rotational Raman lines of nitrogen. The relationship[3] for the temperature T is given by

$$T = H/\ln(R/G)$$

H and G are constants which are determined by the specified transitions used and R is the intensity ratio. The transitions used were the $J = 6$ to $J = 4$ anti-Stokes transition (6, 4), and the $J = 1$ to $J = 3$ Stokes transition (1, 3), where J is the rotational quantum number. These transitions were chosen because they could be easily separated from the remaining Raman spectrum of air and because they provided good temperature sensitivity in the range of interest, 60°–100°K.

To obtain the temperature measurement, a 1 cm^{-1} spectral bandpass was used and the monochromator was positioned on the (6, 4) transition (which is shifted 44 cm^{-1} above the laser line). The intensity of this transition was monitored and the procedure was repeated on the (1, 3) transition (which is shifted 20 cm^{-1} below the laser line). An integration time of 1 sec was used for both the temperature and density measurements.

The density measurements were obtained in two ways: 1) by monitoring the intensity of the vibrational Q-branch of nitrogen, and 2) by using the intensity of the (6, 4) transition. In the first approach, the monochromator was positioned on the Q-branch of nitrogen (which is shifted 2330 cm^{-1} below the laser line) with a spectral bandpass of 10 cm^{-1}. This bandpass was used to eliminate temperature effects on the measured Q-branch intensity over the temperature measurement range. The resulting Q-branch intensity was directly proportional to the gas density and a calibration curve of intensity vs density was established for the static density measurements. In the second approach, the temperature effect on the (6, 4) transition was eliminated by using the measured static temperature to correct the measured intensity of the (6, 4) transition for static temperature variations. This eliminated the temperature dependence, and the resulting intensity of the (6, 4) transition was directly proportional to gas density. By utilizing this second approach for the static density measurements, only two measurements were necessary to obtain static temperature and density: the intensities of the (6, 4) and (1, 3) transitions. In general, however, it is desirable to have temperature and density measurements which are independent—this is the advantage of utilizing the Q-branch intensity to measure static density instead of the (6, 4) intensity.

The calculated temperatures (T_c) and densities (ρ_c) used for comparison were obtained from the local static pressure, total temperature, and total pressure. The static pressure was taken as that measured on the surface of the flat plate below the laser beam. The total temperature is constant throughout the flowfield and the total pressure was determined by assuming the free-stream total pressure undergoes the oblique shock loss associated with the plate angle of attack at the nominal freestream Mach number of 5. The error due to the variation of Mach number with nozzle total pressure is less than 1%. The local Mach number was determined from the ratio of local static to total pressure and the static temperature was determined from this Mach number and the total temperature. The density was then calculated from the static pressure and temperature.

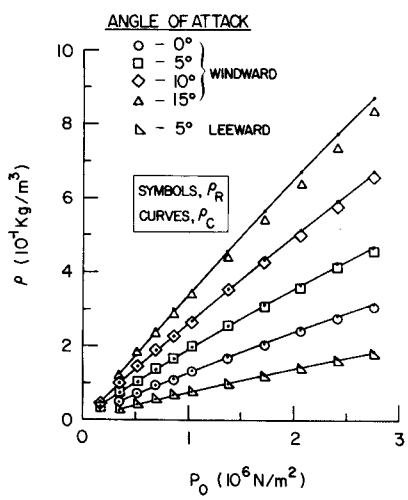

Fig. 2 Static density comparison between measured vibrational Raman values and calculated values.

Results and Discussion

The static gas density measurements based on the intensity of the vibrational Q-branch of nitrogen are compared in Fig. 2 with the density values calculated from measured pressures and temperatures. The static density (ρ) is shown as a function of stagnation pressure (P_o). The Raman density values (ρ_R) are designated by symbols and the calculated density values (ρ_c) by line segments. The standard deviations of the Raman measurements lie within the symbols for this figure and are based on 10 sec of data. In general the agreement between the measured and calculated static density is good throughout the pressure range. The discrepancy at a 15° angle of attack is unexplained but may be associated with errors in calculated local density due to static pressure errors caused by outflow over the plate at this higher angle of attack.

The Raman measurements of static density and temperature obtained by using the pure rotational transitions are shown in Fig. 3. The Raman values of static density obtained from the intensity of the (6, 4) transition are plotted vs the calculated density values (Fig. 3a) and the Raman values of static temperature obtained from the intensities of the (6, 4) and (1, 3) transitions are shown vs the calculated temperatures values (Fig. 3b). The error bars designate one standard deviation based on 10-sec data points and these data were taken at the stagnation conditions $P_o = 3.45 \times 10^5$ N/m^2 and $T_o = 342$°K. The measured density obtained from the rotational transition (Fig. 3a) agrees as well with the calculated values as when the density was determined from the vibrational Q-branch approach. The measured static temperatures (Fig. 3b) also agree well with the calculated values.

Conclusion

The present investigation has demonstrated the capability of the Raman scattering technique to provide local, nonintrusive measurements of static temperature and density in a hypersonic air facility. Static temperatures from 60° to 100°K and static densities from 0.03 to 0.8 Kg/m^3 were measured above a flat-plate model at Mach number 5 over a range of angles of attack (−5° to 15°) and stagnation conditions ($P_o = 1.7 \times 10^5$ to 2.8×10^6 N/m^2 and $T_o = 317°$ to 442°K). The measurement accuracy for static density and temperature of the present investigation shows that Raman scattering offers a viable approach to the measurement problems which exist for high-speed three-dimensional flows.

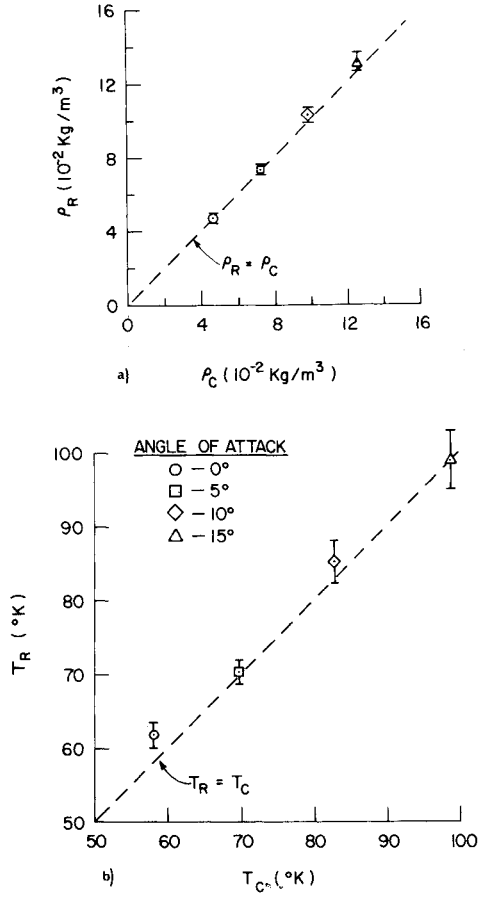

Fig. 3 Static density (a) and temperature (b) comparison between measured rotational Raman values and calculated values.

References

[1] Bandy, A. R., Hillard, M. E., and Emory, M. L., "Evaluation of Raman Scattering as a Sensor of Temperature and Molecular Density," *Applied Spectroscopy*, Vol. 27, No. 6, Nov./Dec. 1973, pp. 421–424.

[2] Widhopf, G. F. and Lederman, S., "Specie Concentration Measurements Utilizing Raman Scattering of a Laser Beam," *AIAA Journal*, Vol. 9, No. 2, Feb. 1971, pp. 309–316.

[3] Salzman, J. A., Masica, W. J., and Coney, T. A., "Determination of Gas Temperatures from Laser-Raman Scattering," TN D-6336, May 1971, NASA.

[4] Penney, C. M., St. Peters, R. L., and Lapp, M., "Absolute Intensity and Polarization of Rotational Raman Scattering from N_2, O_2, and CO_2," CR-121091, Jan. 1973, NASA.

Optimal Scan of the Sky from a Rocket

RUSSELL A. NIDEY*
Kitt Peak National Observatory, Tucson, Ariz.

IN the context of making astronomical measurements by a rocket-launched instrument, McNutt has described a passive system which uses a resonant damper on a spinning rocket[1] to obtain an expanding scan of the sky. Though the resulting scan avoids the unwanted coverage of the ground obtained with simple roll and precession by Friedman and associates,[2] McNutt's scan provides a nonuniform scan rate as well as a nonuniform coverage of the sky. Furthermore, the orientation and pitch of his scan as well as the earlier ones depend upon the specific partition of the angular momentum between the two components. Inasmuch as the transverse component depends upon the time history of the asymmetry of the thrust from the engine as well as that of the aerodynamic restraint, this component is unknowable prior to the flight except in a statistical sense.

With the availability of a computer in an active control system,[3] it is possible in principle to generate any scan including one in which the center of the scan is the zenith, the scan rate is constant, the zenith distance of the axis of the instrument increases linearly with the azimuth distance of the axis of the instrument, and the scan axis is a fixed transverse axis of the instrument. These constraints, by assuring the maximum efficiency in the use of the instrument, a constant information rate from the instrument, a uniform coverage of the sky, and the freedom to use a noncircular field stop in the instrument, respectively, define the optimal scan. The purpose of this Note is to investigate the consequences of these constraints.

Let the instrument assembly be axisymmetric with subscripts λ and τ connoting the axis of symmetry and the scan axis,

Received February 7, 1974. Kitt Peak National Observatory is operated by the Association of Universities for Research in Astronomy, Inc., under contract with the National Science Foundation.

Index categories: Sounding Rocket Systems; Spacecraft Attitude Dynamics and Control.

* Managing Engineer, Rocket Program; present address: NIDEAS, Springfield, Colo. Associate Fellow AIAA.